Available online at www.eccomasproceedia.org
Eccomas Proceedia COMPDYN (2025) 4275-4286

ECCOMAS
Proceedia

COMPDYN 2025
10th ECCOMAS Thematic Conference on
Computational Methods in Structural Dynamics and Earthquake Engineering
M. Papadrakakis, M. Fragiadakis (eds.)
Rhodes Island, Greece, 15-18 June 2025

EXPERIMENTAL ANALYSIS AND FINITE ELEMENT DAMAGE MODELING OF CONCRETE-FILLED STRUCTURAL TUBES SUBJECTED TO PURE BENDING

Rosario Montuori[1], Elide Nastri[1], Vincenzo Piluso[1], Alessandro Pisapia[2], Paolo Todisco[2] and Francesco Fabbrocino[2]

[1] University of Salerno
Via Giovanni Paolo II 132, Fisciano (SA)
r.montuori@unisa.it; enastri@unisa.it; v.piluso@unisa.it

[2] Pegaso Telematic University
Centro direzionale Isola F2, Naples (NA), Italy
paolo.todisco@unipegaso.it; alessandroro.pisapia@unipegaso.it; francesco.fabbrocino@unipegaso.it

Abstract

This study explores experimental testing on eight square concrete-filled tubes (CFTs) with varying width-to-thickness ratios, subjected to both cyclic and constant displacement amplitude under pure bending conditions. Comprehensive finite element modeling (FEM) has been conducted by ABAQUS software to closely replicate the experimental outcomes, focusing particularly on low-cycle damage and failure modes. The simulations incorporated concrete crushing and steel ductile damage, applying an element deletion technique to emphasize material fracture. The FEM results showed strong alignment with the observed cyclic behaviour from the experiments, with an error in energy dissipation under 7%. Lastly, an analytical expression is provided to estimate ultimate parameters (displacement at failure) for FEM applications, offering an effective tool for simulating the hysteretic response of CFTs.

Keywords: CFTs, Steel, Concrete, Experimental, FE simulation.

ISSN:2623-3347
Peer-review under responsibility of the organizing committee of COMPDYN 2025.
doi: 10.7712/120125.127 5.25467

1 INTRODUCTION

Composite structures have gained growing attention due to their excellent stiffness, seismic performance, and fire resistance [1]-[3]. Concrete-Filled Tubes (CFTs), combining a concrete core with a steel tube, offer enhanced structural efficiency by preventing local and global buckling of the steel, outperforming hollow steel sections. Their use is prominent in building columns, especially for large cross sections and bridge piers [4]-[7].

CFT applications are widespread in China, with landmark examples such as the Canton Tower and Zhangmu Railway Bridge [8]. Research has explored steel-concrete interaction mechanisms [9]-[11], and numerous studies have addressed axial capacity through experiments and analytical models [12]-[16]. Specifically, several authors have investigated the effect of the concrete core on local buckling and the axial monotonic/cyclic response of CFTs [17]-[18].

Flexural behaviour under cyclic loading has also been studied extensively for both circular and rectangular sections, focusing on seismic performance and failure mechanisms [19]-[22]. Additional contributions include numerical analyses under biaxial bending [23], shear-bending with concrete damage [24], and hysteretic performance of CFT connections [25],[26]. Lateral impact resistance has been analysed through experimental and numerical approaches [27],[28]. Other studies proposed predictive models for monotonic and cyclic behaviour [29]-[32].

This study addresses a gap in the literature by presenting cyclic bending tests on eight square CFT specimens under constant amplitude. The work is part of a broader experimental campaign at the University of Salerno on CFTs, expanding on prior results for circular sections [33],[34]. The finite element modelling was carried out using ABAQUS (v.2017) [35], accounting for material nonlinearity, concrete crushing, and steel ductility degradation. Experimental data on load-deformation response, failure modes, and energy dissipation were reproduced with high accuracy, with numerical predictions showing less than 7% error in dissipated energy and providing reliable estimates for fatigue life.

2 EXPERIMENTAL CAMPAIGN

The experimental campaign, involved eight square hollow section (SHS) CFT specimens with a length (L) of 2400 mm. The main variable among specimens was the width-to-thickness ratio. Geometric properties: width (B), thickness (t), internal radius (r), are summarized in Table 1.

Each specimen was fabricated from rolled steel sheets, folded and welded longitudinally. Steel end plates (20 mm thick) were welded at both ends, one with a hole for concrete casting. After vertical positioning, specimens were filled with concrete and left to cure. To compensate for minor shrinkage at the top end, a high-strength epoxy resin was applied to ensure a uniform interface between concrete and steel.

	***B* [mm]**	***t* [mm]**	***B/t***
SHS-1	300	7.70	38.96
SHS-2	300	6.10	49.18
SHS-3	300	7.70	38.96
SHS-4	300	6.10	49.18
SHS-5	220	7.80	28.21
SHS-6	220	4.90	44.90
SHS-7	220	4.90	44.90
SHS-8	220	7.80	28.21

Table 1. Geometrical properties

2.1 Mechanical properties

The concrete used corresponds to class C30 ($f_{ck} = 30\ MPa$). During casting, three standard 150 mm cubes were sampled per specimen and tested for compressive strength in accordance with UNI EN ISO 12390-2 [36] ($f_{cm} = 40.83\ MPa$).
Steel mechanical properties were obtained through standard tensile testing as per UNI EN ISO 6892-1-1 [37]. The steel has been classified as S355 [38]. In the following, the mean values of the mechanical parameters are reported: Young's modulus ($E = 206\ GPa$), yield strength at 0.2% strain offset ($f_{0.2} = 437.36\ MPa$), ultimate stress ($f_u = 553.43\ MPa$), strain at maximum stress ($\varepsilon_u = 0.138$), and ultimate fracture strain ($\varepsilon_r = 0.173$) .

2.2 Experimental setup and loading protocol

The experimental program consisted of three-point cyclic pure bending tests, aimed at isolating flexural behaviour. Pure bending is uncommon in practice, it offers a simplified framework to assess material and cross-sectional response, supporting the development of performance-based and seismic design approaches.
As shown in Figure 1, specimens were simply supported over a 3000 mm span using pin-ended hinges, one with a slotted hole to allow longitudinal movement. Flexural loading was applied at midspan via a hydraulic actuator (capacity: 3000 kN compression, 2500 kN tension), connected through a rigid 400 mm stub.

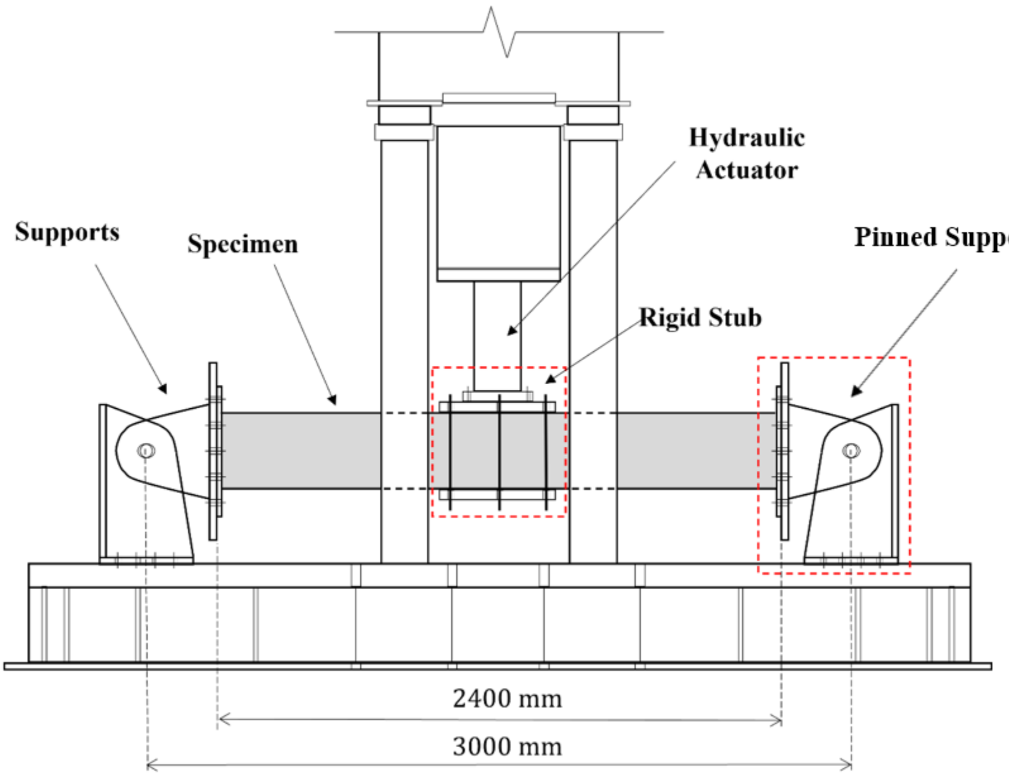

Figure 1. Experimental setup

Instrumentation included LVDTs (1-4) near the ends and upper plates to monitor boundary compliance and ensure negligible fixture deformation. Wire-type displacement transducers were used along the beam to measure the deflected shape.

Specimens SHS-1, SHS-3, and SHS-4 were used as preliminary tests to verify the suitability of the loading protocol and equipment, though their results are also reported for completeness. For specimens SHS-2 and SHS-5 to SHS-8, a displacement-controlled protocol was applied: initially a monotonic loading up to 140 mm, followed by constant-amplitude cyclic loading until either corner fracture with concrete spillage or a 50% drop in load capacity. These tests were designed to investigate low-cycle fatigue behaviour under large displacements and limited cycles to failure.

3 FINITE ELEMENT MODEL

Three-dimensional finite element simulations of the CFT specimens (SHS-2, SHS-5 to SHS-8) have been performed through ABAQUS software [35], employing the explicit solver due to its robustness in handling material and geometric nonlinearities, large deformations, contact interactions, and failure under cyclic loading. The explicit approach has also provided efficient parallel computing and detailed tracking of damage evolution [38],[39].

The FE modelling of CFTs (Figure 2) has required addressing the following key aspects:

Geometric Model and Partitioning:

The models have been constructed using solid elements for the steel tube, concrete core, and end plates. A refined partitioning process has been adopted to enable a structured hex mesh, improving accuracy

Boundary Conditions and Constraints:

Reference points (RP1 and RP2 for supports; RP3 for loading) have been defined and coupled to simulate the test setup. RP1 and RP2 reproduced a hinge and a sliding support, respectively, while RP3 has been assigned displacement control to match the experimental loading protocol

Steel-Concrete Interaction:

Surface-to-surface contact has been defined between the inner face of the steel tube and the concrete core, with a friction coefficient of 0.6 based on prior studies [38]-[42], particularly Tao et al.[41]. A hard contact in the normal direction has been applied to avoid penetration and allow tensile separation.

Meshing Procedure:

C3D8R brick elements with reduced integration have been used. The Element Deletion feature has been enabled for the steel to simulate fracture but disabled for concrete due to contact limitations. A mesh sensitivity analysis has been conducted, considering mesh sizes from 50 mm to 5 mm. Results have indicated that a 30 mm mesh size offers an effective balance between accuracy and computational efficiency.

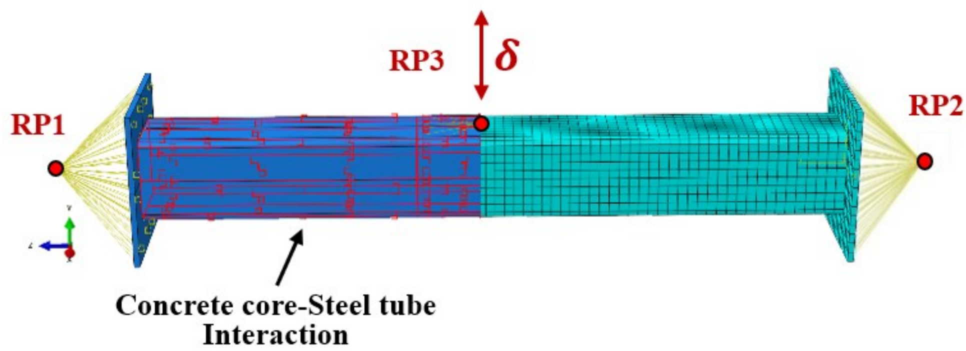

Figure 2. FE model

3.1 Mechanical behaviour: steel

The elastic response has been defined using Young's modulus (E) and the 0.2% offset yield strength ($f_{0.2}$) obtained from tensile tests on dog bone specimens (Section 2.1). For metal plasticity, ABAQUS employs the Von Mises yield criterion with an associated flow rule. A combined isotropic–kinematic hardening model has been calibrated using true stress-strain curves. The backstress evolution is defined by three α_k components governed by parameters C_k and γ_k.

$$\alpha = \sum_{k=1}^{3} \alpha_k \ ; \ \alpha_k = \frac{C_k}{\gamma_k}\left(1 - e^{-\gamma_k \bar{\varepsilon}^{pl}}\right) \tag{1}$$

The adopted values are summarized in Table 6 for each specimen.

Specimen	C_1 [-]	γ_1 [-]	C_2 [-]	γ_2 [-]	C_3 [-]	γ_3 [-]
SHS-2	18000	100	1500	25	380	1
SHS-5	4500	100	5500	26	750	1
SHS-6	19500	220	800	30	350	1
SHS-7	3000	90	2350	25	690	1
SHS-8	17000	200	4900	25	350	1

Table 2. Kinematic hardening parameters

Steel damage has been implemented through the ABAQUS ductile damage function (D), ranging from 0 (no damage) to 1 (complete failure), following the Johnson-Cook (J-C) damage model [59]. The J-C model relates fracture strain $\bar{\varepsilon}_0^{pl}$ to stress triaxiality σ*.

$$\bar{\varepsilon}_0^{pl} = \left[D_1 + D_2 e^{D_3 \sigma^*}\right] \tag{2}$$

Parameters D_1– D_3 have been calibrated based on literature [59] and the experimental dog bone tests reported in section 2.1. The J-C parameters values are shown in Table 3

Specimen	D_1 [-]	D_2 [-]	D_3 [-]
SHS-2	0.010	3.50	-20.03
SHS-5	0.010	10.50	-15.03
SHS-6	0.010	5.50	-19.03
SHS-7	0.025	7.50	-20.03
SHS-8	0.020	4.50	-20.03

Table 3. J-C damage parameters

When the values of $\bar{\varepsilon}_0^{pl}$ and σ^* reach the J-C curve threshold in a mesh element, damage initiates and progresses linearly up to $\bar{\varepsilon}_f$, corresponding to D = 1. The failure displacement $\bar{\delta}_f^{pl}$ depends on the characteristic mesh size L_0 and can be expressed as follows:

$$\bar{\delta}_f^{pl} = (\bar{\varepsilon}_f - \bar{\varepsilon}_0^{pl})L_0 \tag{3}$$

It has been treated as a calibration parameter.
Initial estimates of $\bar{\varepsilon}_f$ were extrapolated from experimental curves and iteratively adjusted to match FE simulation outputs ($\bar{\varepsilon}_{f,FE}$). These values are compared in Table 4.

$\boldsymbol{Specimen}$	$\bar{\varepsilon}_f(D=1)$ [-]	$\bar{\varepsilon}_{f,FE}(D=1)$ [-]
S2	0.21	1.07
S5	0.25	2.55
S6	0.26	2.58
S7	0.25	1.72
S8	0.29	2.90

Table 4. Failure parameters

3.2 Mechanical behaviour: concrete

The mechanical properties of concrete in the elastic range have been defined based on compressive strengths f_{cm}. The undamaged elastic modulus E_0 has been estimated for each specimen using Guo's empirical relation [44]

For plastic and failure behavior, the Concrete Damaged Plasticity (CDP) model has been implemented in ABAQUS, incorporating a modified extended Drucker–Prager yield surface [45],[46] and a non-associated flow rule where the friction angle is replaced by the dilation angle ψ. The required flow rule parameters ψ, eccentricity ε, the biaxial-to-uniaxial compressive strength ratio σ_{b0}/σ_{c0}, and flow stress ratio K have been defined as per recommendations by Lubliner et al. [47] and Lee & Fenves [48], and are listed in Table 5.

ψ [°]	ε [-]	σ_{b0}/σ_{c0} [-]	K [-]
20	0.10	1.16	2/3

Table 5. CDP parameters

Damage in concrete is introduced through tensile cracking and compressive crushing, using stress-strain curves.

The Guo model [44] has been used to define the full stress–strain relationships under uniaxial tension and compression, integrating experimental data through calibrated coefficients. For C30 concrete, the adopted parameters (Table 6) include the peak strain ε_{c1}, and coefficients α_a, α_d.

Strength grade	α_a [-]	α_d [-]	ε_{c1} [10^3]
C30	2.20	0.40	1.40

Table 6. Guo uniaxial parameters

4 RESULTS AND DISCUSSION

The cyclic experimental tests revealed a strong correlation between the width-to-thickness ratio (B/t) and the dissipative performance of the CFT specimens. Specimens SHS-5 and SHS-8, with the lowest B/t ratios (~28.2), exhibited the most stable cyclic behaviour, characterized by delayed flange fracture and minimal strength degradation across cycles. In contrast, specimens with higher B/t ratios (e.g., SHS-6, SHS-7 with B/t = 44.9, and SHS-2 with B/t = 49.2) experienced accelerated degradation, reduced ductility, and lower energy dissipation, confirming the detrimental impact of slender tube walls on cyclic performance.

Additionally, the applied displacement amplitude influenced failure timing, with benchmark specimens subjected to larger displacements collapsing in fewer cycles. Furthermore, SHS-2 despite sharing a similar B/t with SHS-6 and SHS-7 showed higher initial strength due to its larger base (300 mm), but exhibited reduced ductility, suggesting that the volumetric steel-to-concrete ratio also affects the structural response.

Failure modes consistently involved local buckling and bulging of the steel flanges near the rigid stub, coinciding with peak bending moments. Initial bulges formed in compression zones and later mirrored under reversed loading, while minor slips during load reversals were attributed to stub-connection settling. The initial monotonic ramp confirmed that all specimens could sustain large displacements with limited strength loss, indicating high ductility and delayed local buckling phenomena.

Numerical simulations using ABAQUS showed strong agreement with experimental force–displacement hysteresis curves (Figure 3), accurately reproducing key features such as flange bulging and damage localization near the stub (Figure 4). Quantitative comparison in terms of dissipated energy (positive, negative, and total: $E^{(+,-)}$demonstrated good predictive capability of the FEM, with percentage errors in total energy dissipation remaining low (Table 7).

Specimen	$E_{exp}^{(+)}$ [kJ]	$E_{Abq}^{(+)}$ [kJ]	$E_{exp}^{(-)}$ [kJ]	$E_{Abq}^{(-)}$ [kJ]	$E_{exp}^{(tot)}$ [kJ]	$E_{Abq}^{(tot)}$ [kJ]	$e[E^{(tot)}]$ [%]
SHS-2	302.43	297.88	288.59	279.86	591.02	577.83	5.30
SHS-5	531.02	541.37	546.32	523.67	1077.30	1065.00	2.80
SHS-6	172.57	237.22	233.05	215.10	405.62	452.33	5.70
SHS-7	137.29	167.65	166.49	157.11	303.78	324.76	3.30
SHS-8	680.37	706.18	732.81	660.18	1413.20	1367.20	6.50

Table 7. FE and Experimental energy data

Additionally, the cumulative damage function, based on strength degradation per cycle, reached an average of 55% at failure, further validating the accuracy of the simulations.

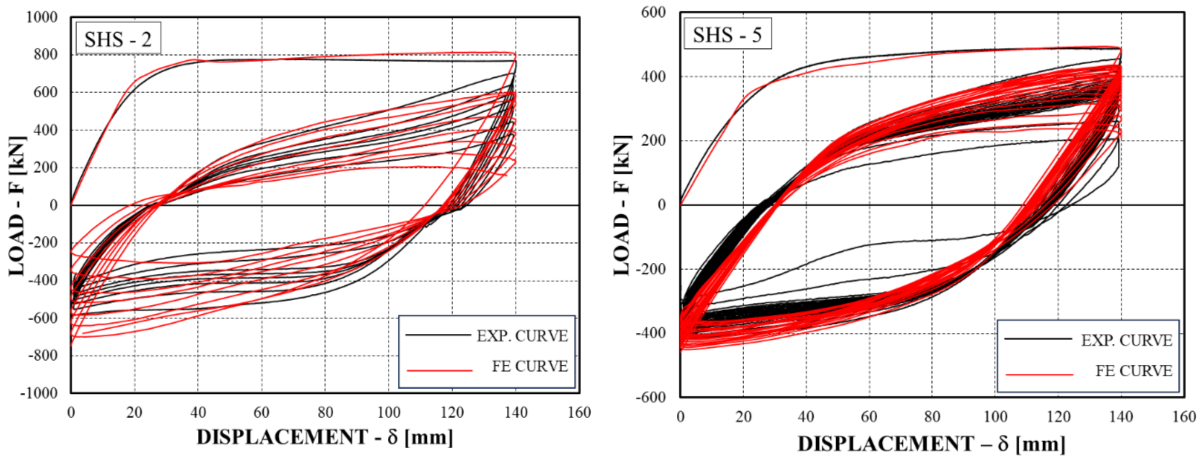

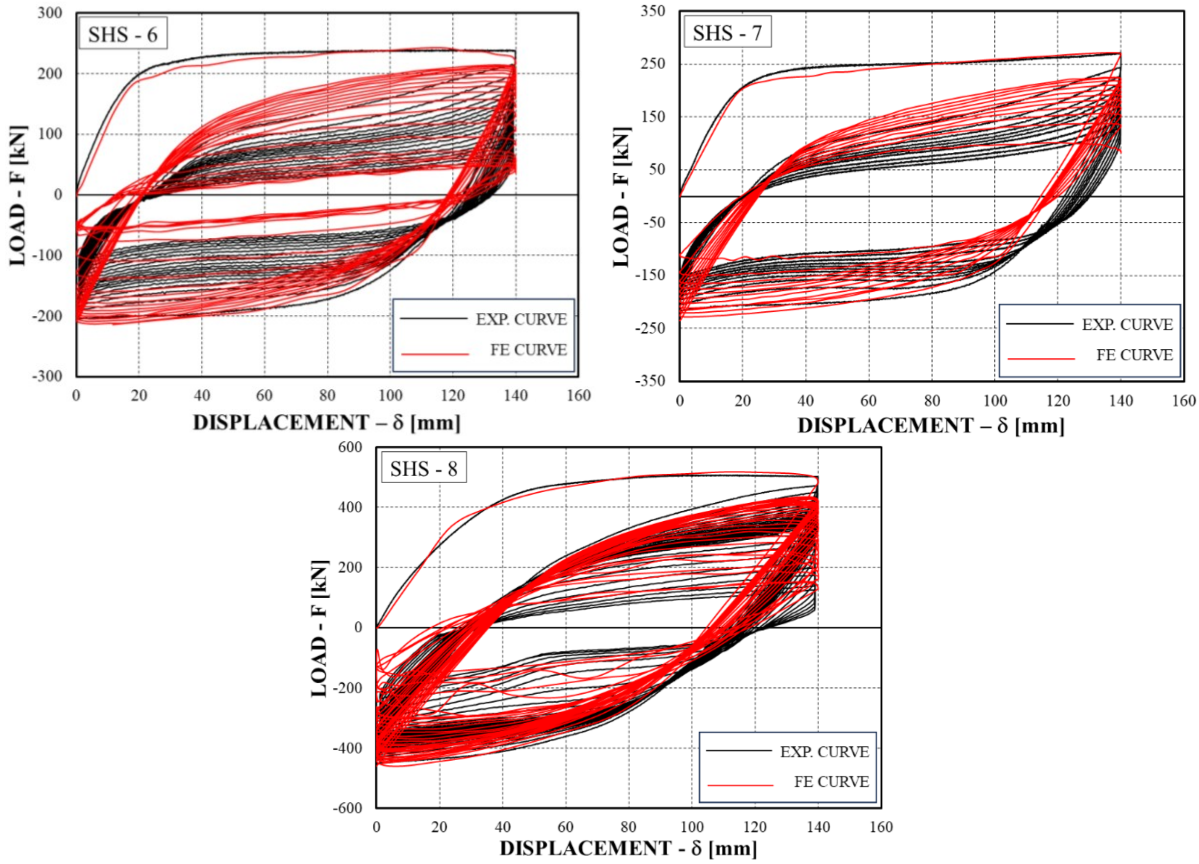

Figure 3. Experimental vs Abaqus curves.

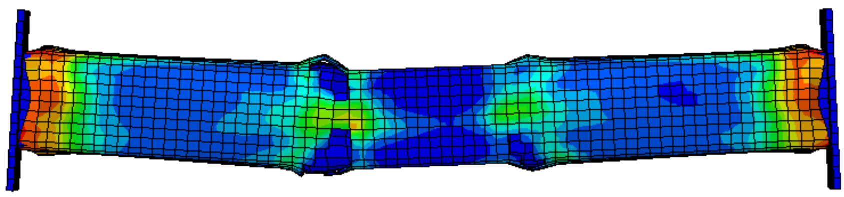

Figure 4. Failure modes.

5 CONCLUSIONS

This study investigated the cyclic behaviour of Concrete-Filled Steel Tubes (CFTs) under constant-amplitude, non-uniform bending. Eight experimental tests were carried out on square hollow sections with varying width-to-thickness (B/t) ratios. A detailed finite element (FE) model was developed and validated through comparison with experimental data, showing good agreement in terms of load–displacement response, failure modes, and energy dissipation.
The results can be summarized in bullets:

- Outward local buckling consistently occurred with a single half-wave deformation pattern.

- Low-cycle fatigue behavior was characterized in terms of force degradation of an average value of 55% at failure.
- CFTs exhibited high ductility, enhanced by the confinement effect of the steel tube on the concrete core.
- Comparison of experimental and FEM-based dissipated energy showed low prediction errors (2.8%–6.5%).

While the number of tested specimens was limited, the framework developed in this work establishes a reliable foundation for future research on the seismic performance and fatigue behavior of CFT structures.

REFERENCES

[1] M. Shams & M.A. Saadeghvaziri: "State-of-the-Art of Concrete-Filled Steel Tubular Columns", *Structural Journal*, 94(5), pp.558-571, 1997.

[2] N.E. Shanmugam & B. Lakshmi: "State of the art report on steel-concrete composite columns", *Journal of Constructional Steel Research*, 57, pp.1041-1080, 2001.

[3] S. Kim, K. Yom, S. Choi: "Evaluation of the fire resistance performance of interior anchor type CFT columns through loaded heating test", International Journal of High-Rise Buildings, 2(1), pp.39-48, 2013.

[4] L.H. Han: "Concrete-Filled Steel Tubular Structures—Theory and Practice", *China Science Press*, Beijing, 2007.

[5] L.H. Han & Y.F. Yang: "Modern Technology of Concrete-Filled Steel Tubular Structures", *China Architecture & Building Press*, Beijing, 2007.

[6] S.T. Zhong: "The Unified Theory of Concrete-Filled Steel Tubular Structures: Research and Application", *Tsinghua University Press*, 2006.

[7] L.H. Han, W. Li, R. Bjorhovde: "Developments and advanced applications of concrete-filled steel tubular (CFST) structures: Members" *Journal of Constructional Steel Research*, 100, pp. 211-228, 2014.

[8] J. Zheng & J. Wang: "Concrete-Filled Steel Tube Arch Bridges in China", *Engineering*, 7(4), pp.143-155, 2018.

[9] J.B. Mander, M.J.N. Priestley, R. Park: "Theoretical stress-strain model for confined concrete", *Journal of Structural Engineering*, 114(8), pp.1804-1826, 1988.

[10] M. Shams & M.A. Saadeghvaziri: "Nonlinear Response of Concrete Filled Steel Tubular Colmuns under Axial Loading", *Structural Journal*, 96(6), pp.1009-1019, 1999.

[11] K.A.S. Susantha, H. Ge, T. Usami: "Cyclic analysis and capacity prediction of concrete-filled steel box columns", *Earthquake Engineering and Structural Dynamics*, 31, pp.195-216, 2002.

[12] D. Lu, Y. Gong, F. Ding, L. Wang, C. Deng, T. Yuan, C. Luo, E. Ren: "Experimental Study of Square CFST Stub Columns with a Low Steel Ratio Under Axial Loading", *Frontiers in Materials*, 8, art.no. 629819, 2021.

[13] J. Yue, H. Fang, Y. Xia, H. Wang, K. Wu: “Damage Evolutions and AE Characteristics for Square Concrete-Filled Steel Tubular Columns Under Axial Load”, *International Journal of Steel Structures*, 20(6), pp.1904-1915, 2020.

[14] Y. Wang, G. Cai, A. Si Larbi, D. Waldmann, K.D. Tsavdaridis, J. Ran: "Monotonic axial compressive behaviour and confinement mechanism of square CFRP-steel tube confined concrete”, *Engineering Structures*, 217, art.no.110802, 2020.

[15] H. Hu, K. Lin, Y. Liu, Z. Guo: “Study on compressive strength of steel tube and concrete in square CFT columns”, *Journal of Building Structures*, 40(2), pp.161-168, 2019.

[16] B. Evirgen, A. Tuncan, K. Taskin: “Structural behavior of concrete filled steel tubular sections (CFT/CFSt) under axial compression”, *Thin-Walled Structures*, 80, pp.46-56, 2014.

[17] Y.Y. Wang, J.P. Liu, B. Wu: “Static and seismic behavior of tubed concrete columns”, *Journal of Harbin Institute of Technology*, 41 (2), pp.38-41, 2009.

[18] S. Ebrahimi, S.M. Zahrai, S.R. Mirghaderi: “Cyclic Performance Evaluation of Hollow Structural Section (HSS) and Concrete-Filled Tube (CFT) Braces”, *International Journal of Structural Stability and Dynamics*, 19(11), art.no.1950140, 2019.

[19] L.H. Han, Y.F. Yang, Z. Tao: “Concrete-filled thin-walled steel SHS and RHS beam-columns subjected to cyclic loading”, *Thin-Walled Structures*, 41, pp.801-833, 2003.

[20] L.H. Han & Y.F. Yang: “Cyclic performance of concrete-filled steel CHS columns under flexural loading”, *Journal of Constructional Steel Research*, 61, pp.423-452, 2005.

[21] X.Y. Mao & Y. Xiao: “Seismic behavior of confined square CFT columns”, *Engineering Structures*, 28 (10), pp. 1378-1386, 2006.

[22] M. Kido, K. Tsuda, T. Fukumoto, Y. Ichinohe, K. Morita: “Limit cycle of square concrete filled steel tubular beam-columns subjected to lateral load with constant cyclic displacement”, *Journal of Structural and Construction Engineering*, 85 (773), pp.981-991, 2020.

[23] J. Liu, X. Zhou, S. Zhang: “Seismic behaviour of square CFT beam-columns under biaxial bending moment”, *Journal of Constructional Steel Research*, 64 (12), pp.1473-1482, 2008.

[24] J. Fujiwara, M. Ohsaki, H. Tagawa, T. Miyamura, T. Yamashita: “Finite element analysis of square concrete-filled-tube column under cyclic shear-bending considering compressive damage of concrete”, *Journal of Structural and Construction Engineering*, 84(755), pp.29-37, 2019.

[25] M.S. Ajith, K.P. Beena, S. Sheela: “Comparative study on hysteretic performance of semi-through connections in CFT beam-column joint”, *International Journal of Engineering and Advanced Technology*, 8(2), pp.48-52, 2018.

[26] M. Wang, & M. Yang: “Experimental Study on Seismic Behavior of Square Concrete-filled Steel Tube Column with End Ribs”, *Journal of Hunan University Natural Sciences*, 44(11), pp. 31-37, 2017.

[27] Gao S., Xu Y.,Zhang S., Derlatka A., Performance of square concrete-filled steel tubular columns under repeated lateral impact, Engineering Structures, Volume 280,2023,115719, ISSN 0141-0296

[28] Shan Gao, Jie Yang, Shao-bo Kang, Fangyi Li, Xiaona Shi, Experimental and numerical studies on deformation performance of square concrete-filled steel tubular columns under repeated lateral impacts, Engineering Structures, Volume 308, 2024, 117909, ISSN 0141-0296

[29] R. Montuori & V. Piluso: "Analysis and modelling of CFT members: Moment curvature analysis", *Thin-Walled Structures*, 86, pp.157-166, 2015.

[30] T. Fukumoto: "Moment-curvature relationship of concrete-filled square steel tube beam-columns under monotonic loading", *Journal of Structural and Construction Engineering*, 84(755), pp.109-118, 2019.

[31] M. Kido, K. Tsuda, M. Haraguchi: "Ultimate strength of concrete filled square steel tubular beam-columns: Required conditions for attainment of full plastic moment and framework and issues of strength design", *Journal of Structural and Construction Engineering*, 85(769), pp.415-425, 2020.

[32] J. Pan, P. Wang, Y. Zheng, Z. Wang, D. Liu: "An Analytical Study of Square CFT Columns in Bracing Connection Subjected to Axial Loading", *Advances in Civil Engineering*, 2018, art. no. 8618937, 2018.

[33] R. Montuori, E. Nastri, V. Piluso, P. Todisco: "Experimental and Analytical Study on the Behaviour of Circular Concrete Filled Steel Tubes in Cyclic Bending", Engineering Structures, 304, art.no. 117610, 2024.

[34] R. Montuori, E. Nastri, V. Piluso, P. Todisco, "Finite element analysis of concrete filled steel tubes subjected to cyclic bending", *Engineering Structures*, Volume 314, 118364, ISSN 0141-0296,2024 https://doi.org/10.1016/j.engstruct.2024.118364.

[35] ABAQUS, 2017. Abaqus/Explicit v. 2017, User's Manual. Hibbit, Karlsson & Sorensen, Inc.

[36] UNI-EN-ISO 12390-2: "Testing hardened concrete - Part 2: Making and curing specimens for strength tests", European Standard, 2020.

[37] UNI-EN-ISO 6892-1: "Metallic materials – Tensile testing – Part 1: Method of test at room temperature", European Standard, 2020.

[38] Montuori R., Nastri E., Piluso V., Pisapia A., Todisco P. Experimental study and finite element damage modelling of concrete-filled structural elements under pure bending (2025) Structures, 74, art. no. 108574, DOI: 10.1016/j.istruc.2025.108574

[39] Nastri E., Piluso V., Pisapia A., Pisciottano F., Todisco P. First exploring the cyclic behaviour of aluminium beams under non-uniform bending: Experimental and FE analysis (2025) Engineering Structures, 322, art. no. 119144, DOI: 10.1016/j.engstruct.2024.119144

[40] L.H. Han, G.H. Yao, Z. Tao: "Performance of concrete-filled thin-walled steel tubes under pure torsion", *Thin-Walled Structures*, 45(1), pp.24-36, 2007.

[41] Z. Tao, Z.B. Wang, Q. Yu: "Finite element modelling of concrete-filled steel stub columns under axial compression", *Journal of Constructional Steel Research*, 89, pp.121-131, 2013.

[42] Z. Lai, J. Yan, Y. Wang, C. Dong, X. Weng: "Axial compressive behavior and design of high-strength square concrete-filled steel tube short columns with embedded GFRP tubes", *Journal of Constructional Steel Research*, 207, art.no.107955, 2023.

[43] M. Murugesan & D.W. Jung: "Johnson Cook material and failure model parameters estimation of AISI-1045 medium carbon steel for metal forming applications", *Materials*, 12(4), art.no.609, 2019.

[44] Z. Guo: "Principles of Reinforced Concrete", *Elsevier*, Oxford, 2014.

[45] E. Nastri & P. Todisco: "Macromechanical Failure Criteria: Elasticity, Plasticity and Numerical Applications for the Non-Linear Masonry Modelling", *Buildings*, 12, art.no.1245, 2022.

[46] R. Montuori, E. Nastri, V. Piluso, P. Todisco: "Experimental and Analytical Study on the Behaviour of Circular Concrete Filled Steel Tubes in Cyclic Bending", *Engineering Structures,* 304, art.no. 117610, 2024.

[47] J. Lubliner J. Oliver, S. Oller, E. Oñate: "A plastic-damage model for concrete", *International Journal of Solids and Structures*, 25, pp. 299–326, 1989.

[48] J. Lee & G.L. Fenves: "Numerical Implementation of Plastic Damage Model for Concrete under Cyclic Loading: Application to Concrete Dam", Report No. UCB/SEMM-94/03; University of California: Berkeley, CA, USA, 1994.

[49] L.S. Jacobsen, "Damping in composite structures", Proceedings of the 2nd world conference on earthquake engineering, no. 2, pp 1029–1044, 1960

[50] Q. Su, G. Cai, H. Cai, Seismic behaviour of full-scale hollow bricks-infilled RC frames under cyclic loads. Bull Earthquake Eng 15, 2981–3012 (2017). https://doi.org/10.1007/s10518-016-0074-6